Biologically Optimized Radiation Therapy

Anders Brahme, Johan Nilsson and Dzevad Belkic

From the Department of Medical Radiation Physics, Karolinska Institutet and Stockholm University, Stockholm, Sweden

Correspondence to: Anders Brahme, Department of Medical Radiation Physics, Karolinska Institutet and Stockholm University, Box 260, SE-171 76 Stockholm, Sweden.

Acta Oncologica Vol. 40, No. 6, pp. 725–734, 2001

Advanced treatment optimization is possible using quantitative radiobiological dose response models. Although all present models are necessarily linked to a certain degree of uncertainty, this will only have a small influence on the relative shape of the resultant optimal dose distribution. However the exact dose level should perferably be determined clinically by dose escalation with the optimized dose plan as a control arm. It is shown that a large part of the biological effect of high linear energy transfer radiation is due to the spectrum of low-energy δ-electrons that can generate dense clusters of complex DNA damage. Such electrons are efficiently generated by low-energy photons or densely ionizing ion beams and to a considerably smaller degree by high-energy electrons, photons and protons. A new analytical expression is developed for the effective radiation resistance of heterogeneous tumors, making it possible to approximate the response of such tumors by the effective clonogen number $N_{0,\mathrm{eff}}$ and the effective D_0 value $D_{0,\mathrm{eff}}$. It is shown that a relatively small number of resistant tumor cells may well be sufficient to dominate the response of hypoxic or otherwise heterogeneous tumors. Finally, several examples are given of intensity-modulated dose distributions generated by multiple radiation modalities, the total effect of which is biologically optimized.

Received 1 December 2000
Accepted 10 January 2001

During the past decade radiation therapy equipment has undergone a significant development, currently permitting advanced three-dimensional intensity-modulated dose delivery to arbitrary tumor volumes anywhere in the human body. The clinical problem with radiation therapy has therefore shifted from sheer dose planning to genuine treatment planning and treatment optimization, taking the radiobiological properties of the tumor and normal tissues into account (1). To make the treatment curative, the internal target volume is generally prescribed a high therapeutic dose. However, the target often overlaps with radiation-sensitive, critical normal tissues, necessitating a local reduction of the dose delivery to ensure a high quality of life. Thus, to find the right balance between cure and complications, radiobiological models that can quantify as accurately as possible the response of heterogeneous tumors and organized normal tissues to non-uniform dose delivery are required for accurate optimization of the treatment outcome. With such models it is possible to find the intensity-modulated dose delivery that within a fraction of 1% maximizes the complication-free cure and at the same time minimizes the risk of inducing severe normal tissue side effects (2).

The interesting mechanism, used by modern radiobiologically based optimization algorithms, is that the dose can be reduced in a small part of the tumor in order to minimize local complications in neighboring sensitive normal structures, provided the dose can instead be increased in other parts of the tumor. The combined total effect is thus at least kept and often even increased, at least in terms of the probability of achieving complication-free cure (3). This is possible since a curative dose which causes 90% tumor control ($P_B \approx 90\%$) also causes on average a clonogenic tumor cell survival $\bar{N}$ of only 0.1 cell since $P_B = e^{-\bar{N}} = e^{-0.1} \approx 0.9$. Hence, if the dose is allowed to increase by about 1 D_0 in, say, half the tumor, so that only 0.02 cells survive there, the dose in the other half may instead be allowed to decrease by almost 1 D_0, so that no more than 0.08 cells would survive there, and still fewer than 0.1 cells will survive on average over the whole tumor. When the dose modifications are only applied in smaller volumes, obviously higher dose modifications are possible and significantly improved complication-free cure is possible by improving the distribution of the highest therapeutic dose levels. In the first approximation, or, more exactly, if the dose variations are small, it is the mean dose to the target tissues which counts and determines the tumor cure (3). Since the mean tumor dose is an important quantity for the response, irrespective of the exact radiation sensitivity of the tumor, intensity-modu-

 ISSN 0284-186X

lated beams can be applied quite generally to improve the treatment outcome for complex tumors (cf. recent reviews (1, 4, 5)). It is even more important to take the properties of the normal tissues into account since most tissues have a fairly parallel organization of their rescuing units and therefore will tolerate local hot spots without significant loss of tissue function (1, 6).

The present study illustrates how this mechanism can also be applied to microscopically heterogeneous tumors and how the new methods can be used for a radiation biology-based optimization of the treatment, particularly if predictive assays are available for estimation of the true sensitivity of the patient at hand.

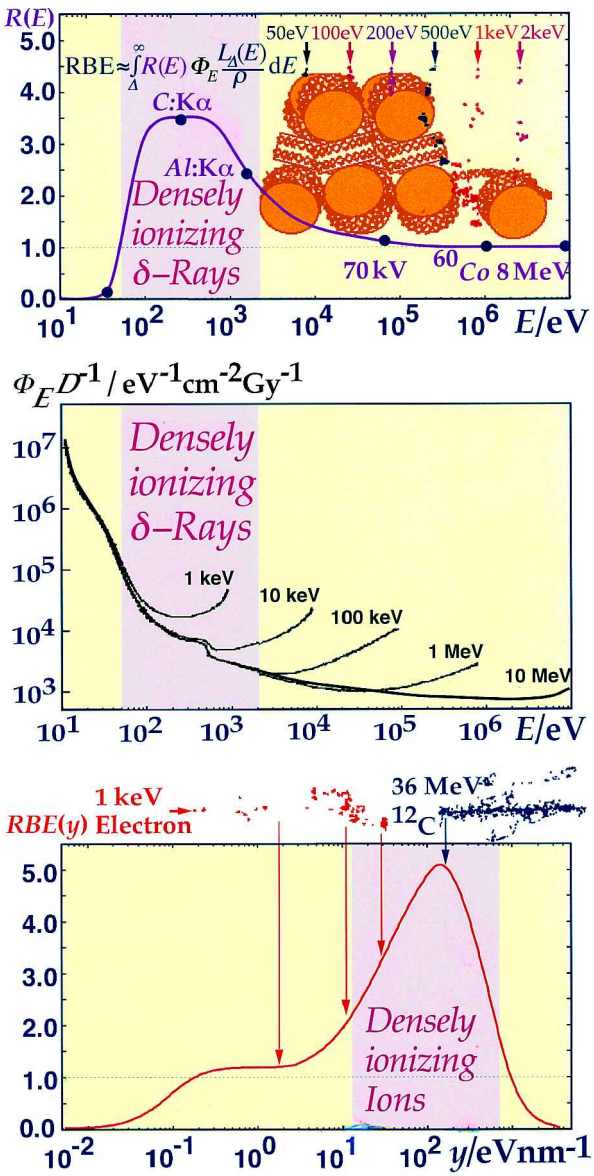

Fig. 1. Illustration of the importance of the low-energy δ-electrons or electron track ends for the relative biological efficiency (RBE) of different radiation modalities from low to high lineal energy (y). The dots on the electron energy response function R(E) in the upper panel are from different experimental RBE values for photons and electrons. The colored electron paths from 50 eV to 2 keV in the upper panel are shown on top of 30 nm DNA fiber (see the text).

CELLULAR MECHANISMS IN TISSUE DAMAGE AND TUMOR ERADICATION

It is customary to describe the variation in the ability of different radiation modalities to eradicate cells by their RBE (relative biological efficiency) as a function of the ionization density or linear energy transfer (LET) of the radiation modality, as illustrated in the lower panel of Fig. 1. It can be seen that at an energy deposition density of around 100 eV/mm, there is a significant peak in the RBE curve largely because, on average, a large number of individual ionizations, each requiring about 30 eV or more, will be deposited over a double-stranded DNA fiber of 2 nm width. However, since at least 80% of the energy depositions are due to secondary electrons—irrespective of the primary radiation type, whether high-energy electrons, photons, protons, neutrons, mesons or ions—it is therefore more natural to describe the biological effect in terms of the associated slowing down spectrum of the electrons, which is shown in the middle panel of Fig. 1, for a set of different initial electron energies. Interestingly enough, the low-energy part of the slowing down spectrum per unit dose to the medium is independent of the initial electron energy as long as it is above some 100 keV, as seen in the middle panel. Indeed this is the reason why high-energy electrons and photons have the same RBE and the absorbed dose is a significant quantifier of radiation effect for these radiation modalities. Protons also essentially belong to this low LET group, since the largest part of the absorbed dose is due to secondary electrons with energies high above the keV range.

When the proton energy reaches the low MeV range, its velocity is close to that of the orbital electrons of the medium, leading to more intense interactions with the medium, thus generating sub keV electrons and therefore a significant high-dose Bragg peak is seen in the depth dose curve. The RBE increases also slightly above unity at this peak (to about 1.3). However, neutrons will set light ions in motion and since ions heavier than protons have a higher charge and therefore a higher ionization density and they generate mainly keV energy secondary electrons that produce dense clusters of ionizations with a high biological efficiency, as shown by the inserted tracks in the lower panel of Fig. 1. A more functional description of the biological effect of different radiation modalities is therefore obtained from the dependence of the biological effect on the energy of the secondary electrons, as shown by the top panel of Fig. 1. Below some 30 eV the electrons do not do much harm because they cannot ionize. However, from 100 eV to about 1 keV the electrons are associated with

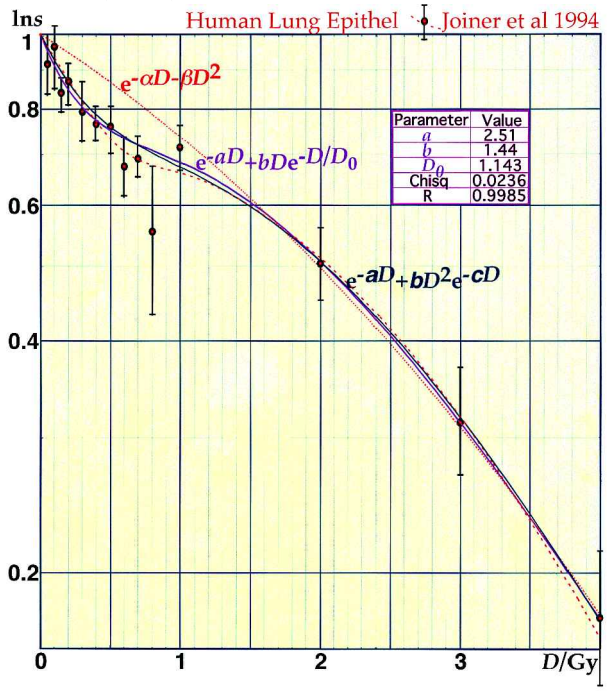

Fig. 2. Comparison of different cell survival models fitted to experimental human lung epithelial cell response (13). The simple bi-exponential expression in Equation [1] gives a good fit over the entire dose range, whereas the a- LQ model is only useful around a few Gy per fraction in dose delivery. The first term of the bi-exponential expression corresponds to lethal irreparable cell kill, whereas the second term describes the sublethal repairable damage, which is shown as being fully repaired in the figure.

very dense ionization clusters with an RBE of around 3. As the electron energy is increased above this range, a decreasing portion of the energy deposition is in the form of such low-energy densely ionizing δ-electrons.

Even if the main radiobiological characteristics of different radiation modalities are linked to the energy distribution of the secondary electrons, there are also other factors that influence the RBE. With increasing atomic number of the ion, the density of low-energy δ-electron production increases so that multiple δ-rays per nm are produced. This causes many of the generated radicals to recombine with each other before they have a chance to damage DNA, thus reducing the RBE at the highest LETs beyond about 200 eV/nm. Furthermore, a small fraction of the energy deposition is due to direct ion recoils but most of that energy has also to pass through low-energy δ-rays before it is finally thermalized. It is thus clear that the shape of the energy spectrum of low-energy δ-electrons will be fundamental for the radiobiological properties of different radiation modalities, as illustrated in Fig. 1 and discussed at a recent microdosimetry meeting ((7), see also (8–10)).

From the above discussion, it is clear that there is a spectrum of DNA lesions from the most severe clusters generated by sub keV δ-electrons to the sparse ionizations by high-energy electrons and their associated oxygen radical-mediated damage. The latter will to a large extent generate sublethal damage that can be repaired if appropriate conditions prevail after irradiation. It can readily be shown that the more severe irreparable damage causes a pure exponential cell survival (11). If the sublethal damage is allowed to be fully repaired, the repaired fraction will be proportional to the dose at low doses, whereas at high doses it also becomes quasi-exponential, as might be expected based on binomial or Poisson statistics grounds (12).

If the appropriate conditions for repair of sublethal damage prevail, the cell survival may therefore be approximated by the following bi-exponential expression:

$$s(D) = e^{-aD} + bDe^{-D/D_0} \quad [1]$$

where the first term describes the irreparable cell kill characterized by the radiation sensitivity a (11) and the second term describes the increased survival as a result of repairable sublethal damage. As seen in Fig. 2, this expression adequately describes the cell survival at both low intermediate and high doses, whereas the classical linear quadratic expression is good only at intermediate doses around a few Gy. Based on Equation [1], it is tempting to think that cell survival is a deterministic process as a function of dose. However, to treat the real cell survival accurately, each cell should be followed separately and the total cumulative effect is that due to the effect on all cells. Each cell can either die ('0') or survive ('1') so that the cell survival is essentially a binomial process where 0 or 1 is the only end point for each cell. The probability distribution of cell survival is thus given by the binomial expression in Fig. 3. At zero dose all cells are alive as given by the sharp peak (barely visible at $P_v = 1$ and $\ln s = 0$) at the origin in the figure. When the dose in increased, the probability distribution is spread out as expected due to the laws of statistics. The interesting fact is now that at high doses the probability again reaches unity when practically all cells are hit and the probability of having no surviving cells is almost unity or 100%. If the cells were tumor clonogens, this would be identical to total tumor eradication and thus 100% probability of tumor cure or a beneficial treatment ($P_B = 1$). Fig. 3 therefore illustrates how the cell survival curve at low doses is transformed to a dose response relation for tumor control at high doses by binomial statistics. Within the limit of a very large number of cells, the binomial expression is well approximated by the Poisson expression, according to which:

$$P_B = e^{-\bar{N}} = e^{-N_0 s(D)} \quad [2]$$

A similar relation may also be used for the normal tissues but then N signifies the number of functional subunits that should largely be left intact in order not to lose tissue function (6, 14). Since the binomial equation in Fig. 3 is based on the assumption of a uniform distribution of

radiation sensitivity, it still must be regarded as a simplification. In fact, since hypoxia is an essential phenomenon in most tumors, it is likely that there is a whole distribution of radiation sensitivities as illustrated in the middle panel of Fig. 4 and described by the distribution function of radiation resistance: n_{D_0}, the integral of which is the total number of cells according to:

$$N_0 = \int_0^\infty n_{D_0}\, dD_0 \qquad [3]$$

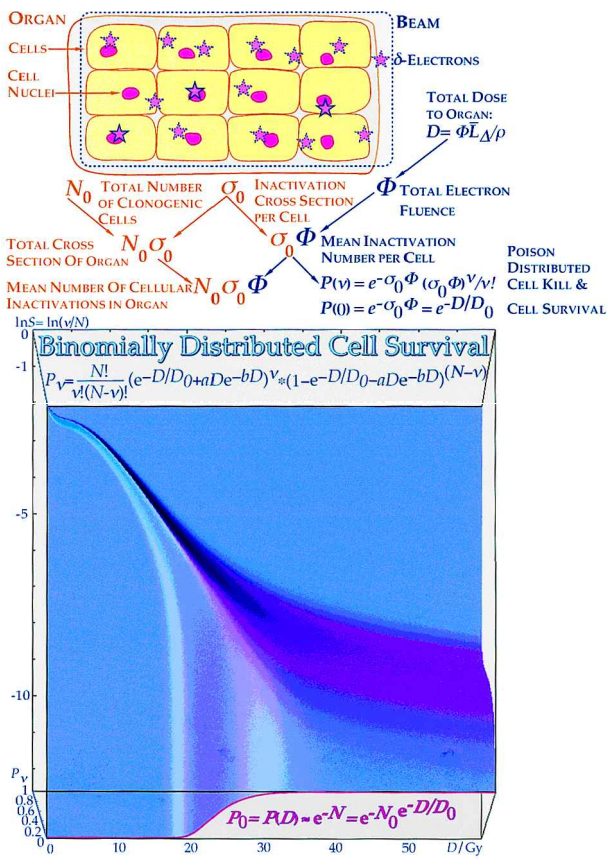

Fig. 3. The interaction of the δ-electrons from a radiation beam with the cell nuclei of a small section of tissue or tumor cells. The binomial cell survival is bi-exponential at low doses and changes to an essentially sigmoidal dose response curve at low survival levels and high doses. The data are taken from the human lung epithelial cells in Fig. 2.

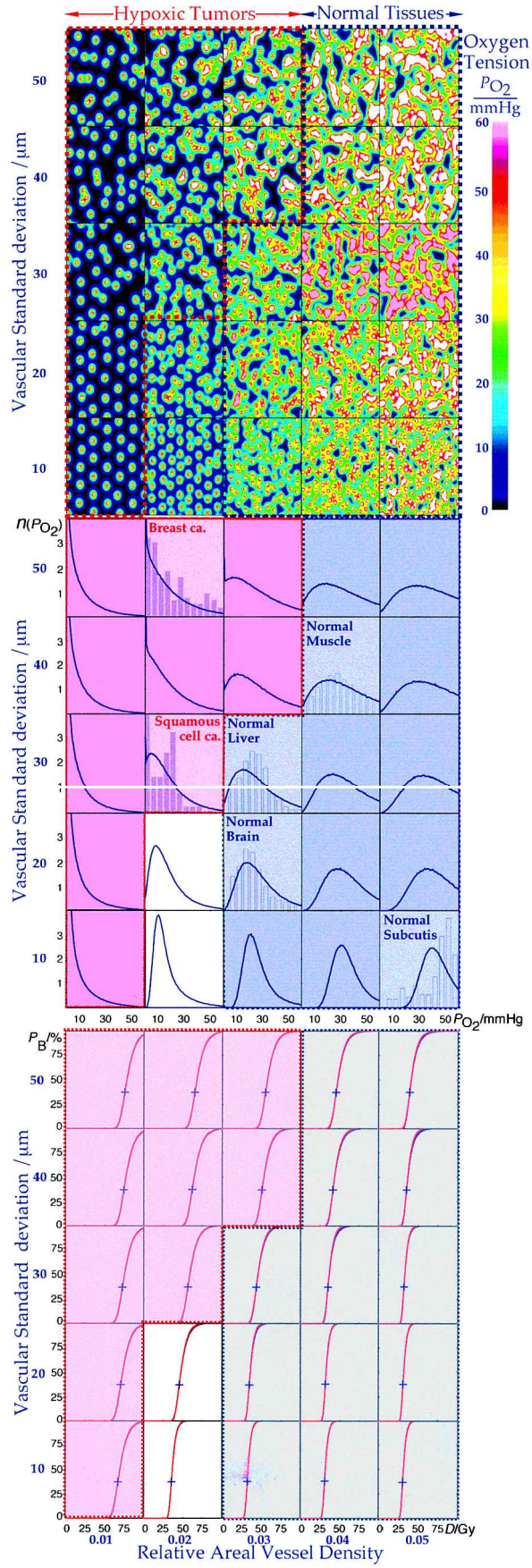

Fig. 4. Schematic comparison of cellular oxygenation distributions (upper and middle panels) and associated dose response curves (lower panel) for different tissue models with increasing vessel density and variation in vascular structure (upper panel). It is seen that the tissue model agrees fairly well with clinically observed oxygenation distributions both for hypoxic tumors (pink-red shading) and well-oxygenated normal tissues (blue shading). It is clear that the hypoxic tumors are more radiation resistant than the well-oxygenated normal tissues, as seen by their lower D_{37} values (+) in the bottom panel. Equally located diagrams correspond to the same tissue structure in these $5 \times 5 = 25$ regions of different vascular characteristics.

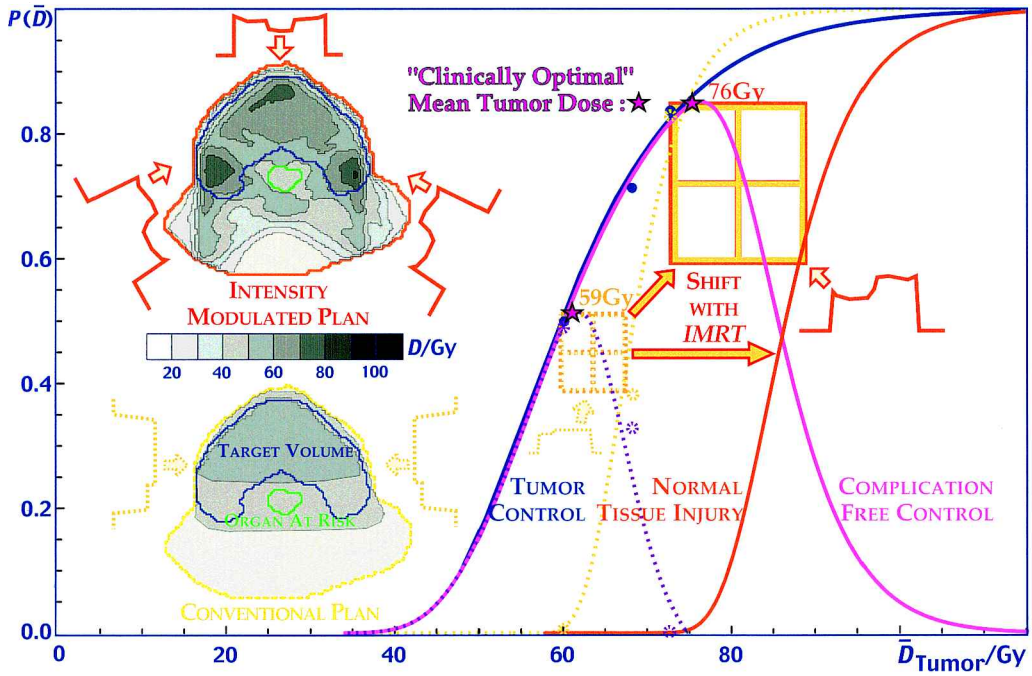

Fig. 5. Comparison of the dose response relations for quasi-uniform and intensity-modulated dose delivery. The increase of the therapeutic window between tumor cure and normal tissue damage with intensity-modulated dose delivery is clearly seen. The shift in the complication curve (orange) and the increase in complication-free cure (violet) are due to the increased dose to the tumor and decreased dose to the spinal cord as the intensity-modulation is introduced. The mean tumor dose is plotted on the horizontal axis so that the complication curve moves to higher doses but the tumor control curve remains unchanged, thus increasing the therapeutic window and the complication-free cure.

The tumor cell distribution n_{D_0} is differential in D_0 and thus describes the degree of variability in radiation resistance of a tumor or normal tissue. The upper panel of Fig. 4 illustrates how a simple tissue model with different vessel densities and degrees of vascular heterogeneity can be used to calculate distributions of partial oxygen pressure (middle panel cf. 15) and for comparison clinically measured oxygen distributions using Eppendorf electrodes (16) are also included.

Interestingly enough, it is possible to approximate the true heterogeneous response by a simple exponential cell survival as a function of the dose D as given by:

$$N(D) = \int n_{D_0} s(D)\, dD_0 \approx N_{0,\mathrm{eff}} \cdot e^{-D/D_{0,\mathrm{eff}}} \qquad [4]$$

where the last approximate expression for $N(D)$ is characterized by a single exponential expression with the effective cell number $N_{0,\mathrm{eff}}$ and effective D_0 value $D_{0,\mathrm{eff}}$. By ensuring that this expression is equal to $N(D)$ at the dose of interest D and, furthermore, that the rate of cell loss at dose D equals the true value given by the derivative of the first exact part of Equation [4], we obtain

$$D_{0,\mathrm{eff}}(D) = \frac{\int n_{D_0} s(D)\, dD_0}{\int n_{D_0} \dfrac{\partial s(D)}{\partial D}\, dD_0} \qquad [5]$$

which is the effective radiation resistance of the cell population at dose D. As shown in the lowest panel of Fig. 4, this expression alone also accurately expresses the dose response relation for highly heterogeneous or hypoxic tissues (15). A particularly important value of $D_{0,\mathrm{eff}}$ is at the dose where the effect probability is $1/e$ or 37%, that is where $N(D_{37}) = 1$ according to Equation [2]. If we, for simplicity, assume that the cell survival is purely exponential (cf. Equation [4]), this clinically most interesting value is given by:

$$D_{0,\mathrm{eff}}(D_{37}) = 1 \Big/ \int \frac{n_{D_0}}{D_0} e^{-D_{37}/D_0}\, dD_0 \qquad [6]$$

which clearly shows that a few resistant or hypoxic cells with high D_0 values may totally dominate the response of a tumor. From Equation [4] we can also derive the effective initial clonogen number according to:

$$N_{0,\mathrm{eff}} = N(D) e^{D/D_{0,\mathrm{eff}}} \qquad [7]$$

which is significantly lower than the real initial cell number $N(0)$ according to Equation [3]. Since the normalized slope of the dose response relation is proportional to the logarithm of $N_{0,\mathrm{eff}}$ it will be reduced relative to a uniform cell population. Again, this value will be particularly important at the steepest point of the dose response curve, close to D_{37} (15). In the lower panel of Fig. 4 the dose response

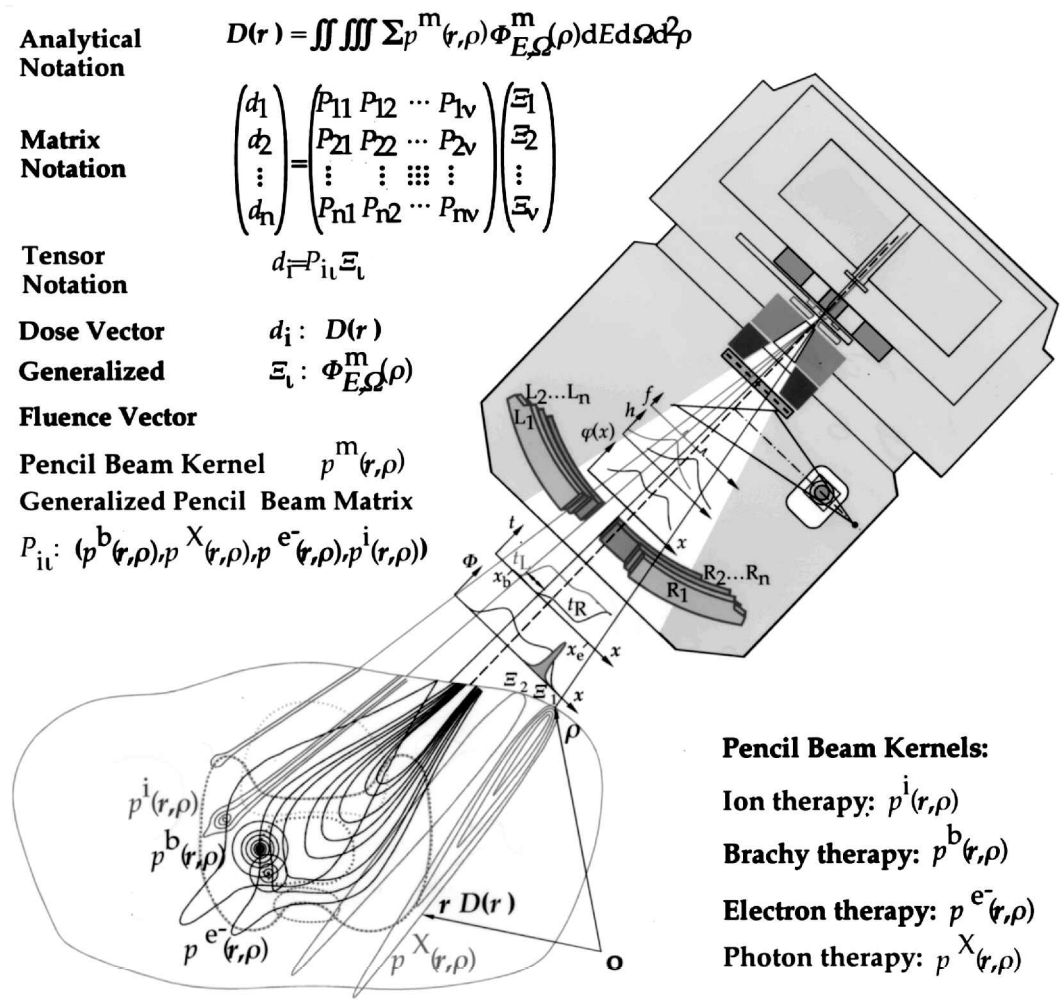

Fig. 6. Illustration of intensity-modulated dose delivery using multiple pencil beams or point source energy deposition kernels. For each pencil beam energy deposition kernel component, the optimal fluence weight Ξ is selected, so that the complication-free cure is maximized. In the analytical notation, an inverse integral, or the so-called Fredholm equation, is obtained, whereas in the matrix formulation a matrix inversion is required.

relations obtained from the cellular distribution functions in the middle panel of Fig. 4 are obtained using the more exact first half of Equation [4] (solid curves) as well as the approximate last half (dashed curves). As seen in the lowest panel of the figure, there is a negligible difference between the two dose response relations in each case.

The shape of the resultant dose response relation both for heterogeneous and uniform tissues is sigmoidal, as shown in the lower part of Fig. 3. However, for heterogeneous tumors and normal tissues, the slope of the dose response relation is lower and therefore higher doses are required to cure the tumor and lower doses are often tolerated less well by the normal tissues. An important task in clinical radiation therapy is to quantify the shape of the dose response relation based on the treatment outcome in terms of both tumor cure and normal tissue injury and the desirable outcome in complication-free cure. It is also essential to quantify the correlation between these outcome measures, since it is of fundamental importance for the maximization of the complication-free cure (17). Today a substantial amount of clinical data is rapidly becoming available (1, 4, 5, 14, 18–22) making it possible to perform a more strict treatment optimization also for more complex tumor and normal tissue configurations (1).

RESULTS

A first clinical example is presented in Fig. 5, illustrating the significant therapeutic advantages achieved by using biologically optimized intensity-modulated radiation beams (1, 4). Fig. 5 compares the same central slice and isodose diagram through a head and neck target with a quasi-uniform classical and an intensity-modulated beam treatment and the associated dose response curves for the two treatments. This treatment configuration allows a clear-cut comparison of the two treatment techniques since the common dose axis is in units of the mean dose to the tumor or, more exactly,

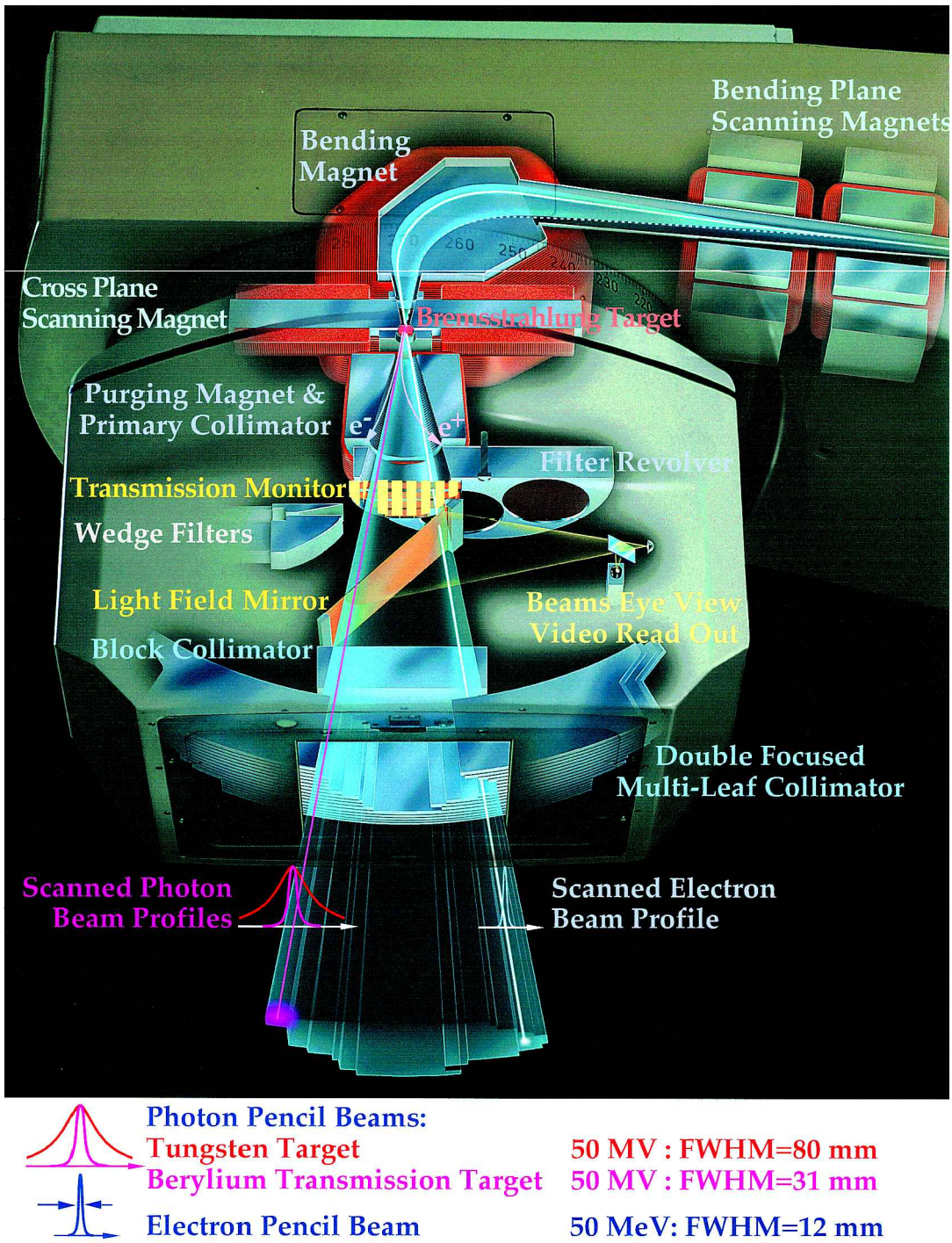

Fig. 7. Cross-section through the treatment head of an advanced treatment unit for intensity-modulated radiation therapy. Through the design of the scanning system both narrow photon and pencil electron beams can be produced and scanned across the patient to produce arbitrary dose distributions in the tumor. At all times the multileaf collimator protects normal tissues outside the tumor, whereas the intensity-modulation allows longitudinal protection of normal tissues in front of, behind and even inside the tumor volume.

to the internal target volume. Therefore, the dose response curves for the tumor will be practically the same in the two cases (left-most blue solid sigmoidal curve). However, the normal tissue complication curves are different, since in the intensity-modulated plan (solid orange curve) the dose to the tumor is significantly increased while the dose to the critical normal tissues is slightly reduced. All curves are related to the mean tumor dose, and since this has increased over the normal tissue dose by about 10 Gy compared to the plan with essentially uniform dose delivery, the solid complication curve for the intensity-modulated plan has moved by about 10 Gy to the right from its

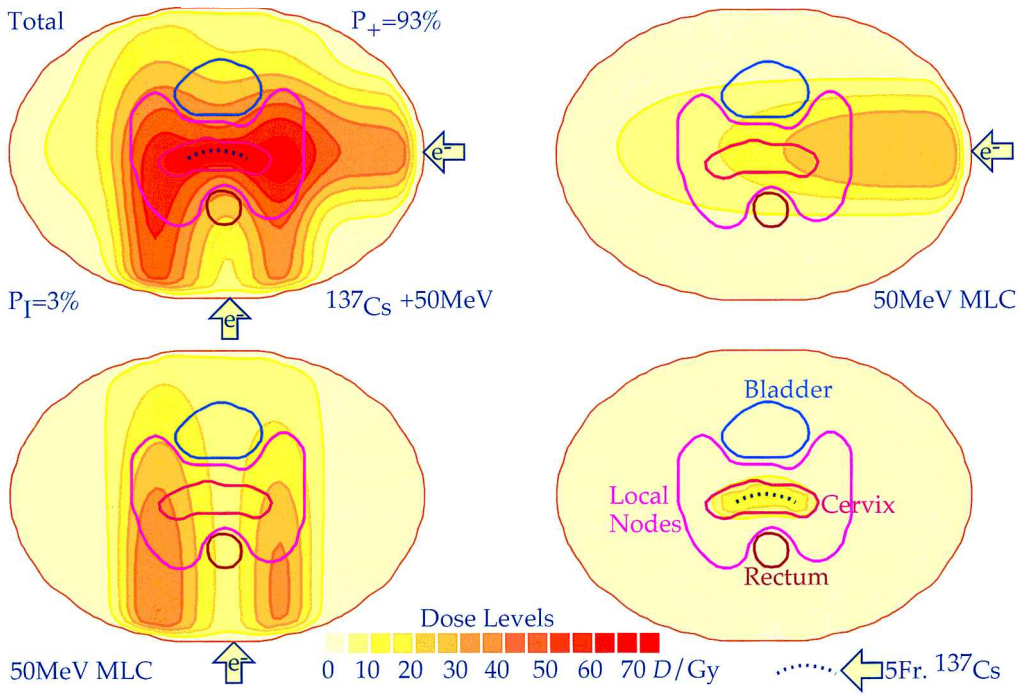

Fig. 8. Optimization of external electron beam therapy combined with pulsed intracavitary brachytherapy. It is seen how the combined dose distribution protects the rectum and bladder at the same time as a high therapeutic dose is delivered to the cervix and the locally involved lymph nodes.

location in relation to essentially uniform dose delivery (dotted sigmoidal curve). As a consequence, the therapeutic window has opened up substantially, and the bell-shaped curve for complication-free cure (P_+) has increased from about 50% to 85%. This significant increase in treatment outcome is achieved because biologically optimized intensity-modulated dose delivery results in an increased dose to the tumor at the same time as the normal tissues are spared to a greater extent. This also implies that the classical double trouble problem in dose escalation is converted to a double advantage. Not only is the relative dose to the normal tissues reduced, but the dose per fraction is also diminished, as is the risk for severe late complications. This simple comparison thus clearly presents the overall advantages that can be achieved by biologically optimized intensity-modulated dose delivery.

The widening of the therapeutic window in Fig. 5 was achieved through a biologically optimized intensity-modulation so that the peak of the complication-free cure curve (P_+) is reached. The intensity-modulation is further illustrated in Fig. 6, where a set of different narrow pencil beam kernels from photons and electrons to brachytherapy and ion beams are shown. During the optimization process, the optimal weight of each pencil beam is determined in such a way that the resulting total dose distribution maximizes the complication-free cure (P_+) of the treatment. This problem is nowadays sometimes solved as an inverse problem attempting to find the generalized fluence vector, which generates the desired dose distribution in the patient. However, looking at this problem as a biological treatment optimization challenge is even more fruitful, since one can find not only the optimal fluence but also the associated dose distribution which indeed maximizes the treatment objectives such as the complication-free cure, P_+ (cf. Fig. 5).

Fig. 6 also schematically illustrates how the intensity-modulated dose delivery is achieved either by dynamic multileaf collimation, by the narrow, scanned pencil beam or by both of these processes simultaneously. The scanned beams are shown more clearly in the exploded view of the treatment head of a modern treatment unit in Fig. 7, where the bending plane and cross plane scanning magnets can deflect the electron beam to an arbitrary position in the patient. In the photon mode, a target is inserted after the last scanning magnet so that the generated bremsstrahlung continues as a narrow lobe in the direction of the deflected electrons. In this way the narrow electron and photon beam can be deflected anywhere in the patient plane to intensity-modulate the resultant broad electron or photon beam. The multileaf collimator can then be configured to protect normal tissues lateral to and surrounding the tumor, whereas the intensity-modulation is done to protect normal tissues longitudinal to, in front of, behind and even inside the tumor. The treatment head also includes a beam's eye view video monitor and a high field strength purging magnet to allow observation of the exact

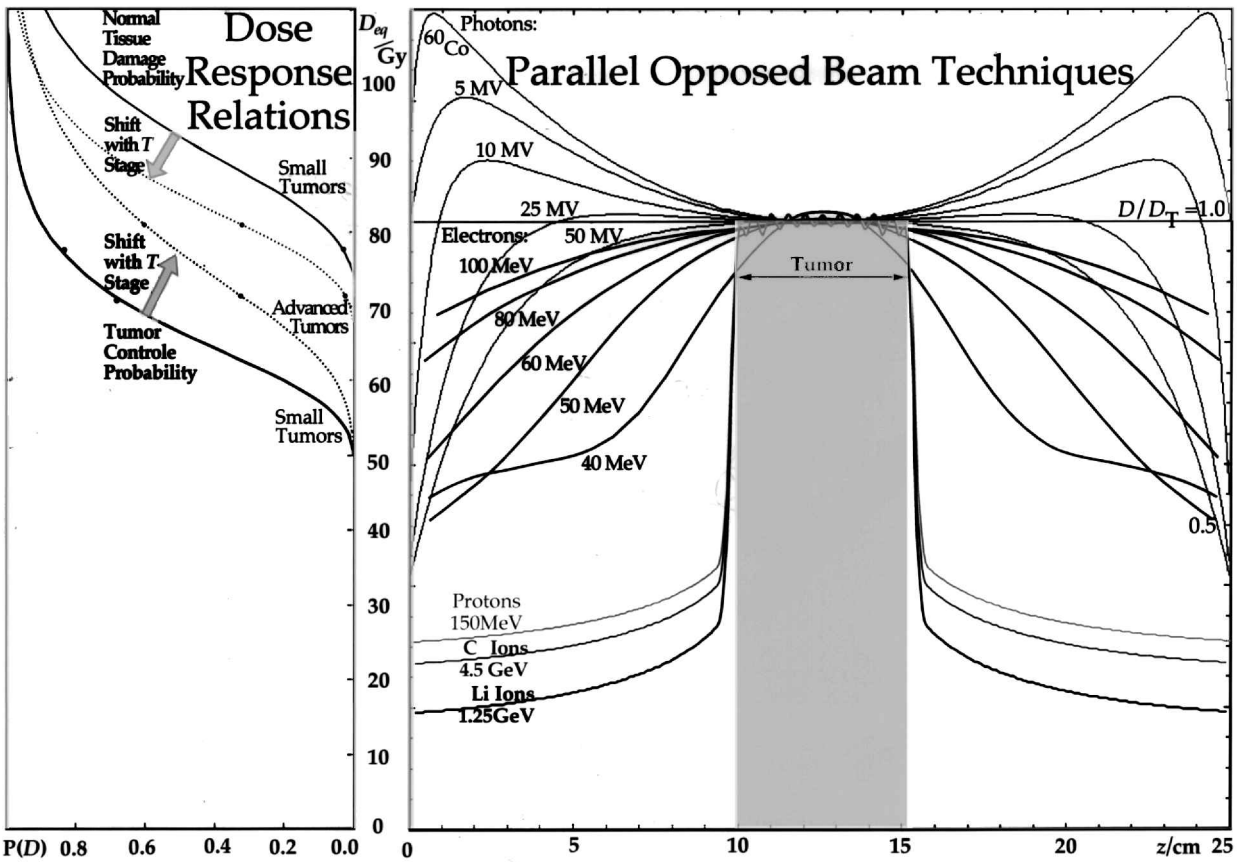

Fig. 9. Comparison of different radiation modalities from photons and electrons to protons and light ions for the treatment of a pelvic tumor by parallel opposed beam techniques. It can be seen that the dose to the normal tissues is continuously decreased as the energy is increased for photons and brought to the 40–50 MeV range for electrons. The light ions (Lithium–Carbon) are most advantageous because of their increased biological effect in the Bragg peak. From the dose response curves along the vertical dose axis, it can be seen that the electrons and ions should not produce any severe normal tissue damage, even though late appearing damage would be lower with the ion beams.

collimator setting and to remove the electron contamination produced by the photon beam.

According to Fig. 6 multimodality intensity-modulated dose delivery can be used to optimize fairly complex treatments. Fig. 8 illustrates how the scanning pattern of the electron beam can simultaneously be optimized together with the motion pattern of a pulsed brachytherapy source (dashed line) so that the total dose delivery in the upper left corner maximizes the total complication-free cure. It is clearly seen how the algorithm combines the scanned electron beam dose delivery with the intracavitary source motion pattern in the lower right diagram. As seen in Fig. 8, about one quarter of the dose is delivered by brachytherapy, whereas the remainder is shared almost equally between the two electron beams. Good shielding of the bladder and rectal volumes is clearly seen. This certainly shows the power of biological optimization where different radiation modalities can be combined in an optimal way. This can be done using multiple electron or photon energies or even the best combination of low and high LET beams (1).

Finally, Fig. 9 illustrates how different radiation modalities can be used in parallel opposed beam configurations to treat a deep-seated tumor such as a bladder or prostate cancer. An interesting aspect of this treatment is that it allows a clear-cut comparison of different radiation modalities in one and the same beam configuration. It is seen that for this deep treatment, low to medium energy photons are not sufficient owing to excessive doses in shallow tissues. The highest photon energy (50 MV) is quite useful, whereas 25 MV is marginally useful and the high-energy electrons, especially those around 40–60 MeV, are most useful among the classical radiation modalities for this kind of target volume and treatment technique. Using protons and light ions will allow a considerable reduction of milder treatment-related side effects in the normal tissues, as seen by the considerably reduced biological effect in the ion beam cases. However, in this case only the RBE at the Bragg peak was used to calculate the biological effective dose distribution for the ion beams. Lithium and carbon ions also have a significantly lower oxygen enhancement ratio than electrons, photons and protons.

Therefore, one would expect an even better therapeutic result with these beams for the hypoxic tumors that today are known to be overwhelmingly encountered in the clinic, as could be inferred from Fig. 4.

ACKNOWLEDGEMENTS

The invaluable support of the Research Center for Radiation Therapy by The Swedish National Board for Industrial and Technical Development and the continued stimulation by all its members and the researchers at the Department of Medical Radiation Physics are gratefully acknowledged.

REFERENCES

1. Brahme A. Development of radiation therapy optimization. Acta Oncol 2000; 39: 579–95.
2. Löf J. Development of a general framework for optimization of radiation therapy. PhD thesis, Dept of Medical Radiation Physics, Stockholm University and Karolinska Institutet, 2000.
3. Brahme A. Dosimetric precision requirements in radiation therapy. Acta Radiol Oncol 1984; 23: 379–91.
4. Tubiana M, Eschvège F. Conformal radiotherapy and intensity-modulated radiotherapy. Acta Oncol 2000; 39: 555–67.
5. Withers HR. Biological aspects of conformal therapy. Acta Oncol 2000; 39: 569–77.
6. Källman P, Ågren A, Brahme A. Tumor and normal tissue responses to fractionated non uniform dose delivery. Int J Rad Biol 1992; 62: 249–62.
7. Brahme A, Rydberg B, Blomquist P. Dual spatially correlated nucleosomal double strand breaks in cell inactivation. In: Goodhead DT, Menzel ONeill P, '' HG, eds. Microdosimetry. An interdisciplinary approach. Cambridge: The Royal Society of Chemistry, 1997: 125–8.
8. Tilikidis A, Brahme A. Microdosimetric description of beam quality and biological effectiveness in radiation therapy. Acta Oncol 1994; 33: 457–69.
9. Folkard M, Prise KM, Vojnovic B, Davies S, Roper MJ, Michael BD. Measurement of DNA damage by electrons with energies between 25 and 4000 eV. Int J Radiat Biol 1993; 64: 651–8.
10. Michalik V, Frankenberg D. Simple and complex double-strand breaks induced by electrons. Int J Radiat Biol 1994; 66: 467–70.
11. Brahme A, Ågren A. On the optimal dose distribution for eradication of heterogeneous tumors. Acta Oncol 1987; 26: 377–85.
12. Lind BK, Nilsson J, Löf J, Brahme A, Generalization of the normalized dose response gradient to nonuniform dose delivery. Acta Oncol 2001; 6: 718–24.
13. Singh B, Arrand JE, Joiner MC. Hypersensitive response of normal human lung epithelial cells at low radiation doses. Int J Radiat Biol 1994; 65: 457–64.
14. Withers HR, Taylor JMG, Maciejewski B. Treatment volume and tissue tolerance. Int J Radiat Oncol Biol Phys 1988; 14: 751–9.
15. Nilsson J, Lind BK, Brahme A. The radiation response of hypoxic and generally heterogeneous tissues. Int J Radiat Biol 2000; In press.
16. Vaupel P. Oxygenation of human tumors. Review article. Strahlenther Onkol 1990; 166: 377–86.
17. Ågren A, Brahme A, Turesson I. Optimization of uncomplicated control for head and neck tumors. Int J Rad Oncol Biol Phys 1990; 19: 1077–85.
18. Rubin P. A direction for clinical radiation pathology. The tolerance dose. In: Vaeth JM, ed. Front radiation therapy and oncology. Basel, Switzerland: S Karger, 1972: 1–16.
19. Thames HD, Hendry JH. Fractionation in radiotherapy. London: Taylor & Francis, 1987.
20. Emami B, Lyman J, Brown A, et al. Tolerance of normal tissue to therapeutic irradiation. Int J Radiat Oncol Biol Phys 1991; 21: 109–22.
21. Ågren Cronqvist AK. Quantification of the response of heterogeneous tumours and organized normal tissues to fractionated radiotherapy. Thesis, Dept Medical Radiation Physics, Stockholm University, 1995.
22. Brahme A. Biologically based treatment planning. Acta Oncol 1999; 38 (Suppl 13): 61–8In: Mustakillio Centennial Symposium Helsinki.